

See discussions, stats, and author profiles for this publication at: <https://www.researchgate.net/publication/50302841>

The (CH₂)₂O-H₂O Hydrogen Bonded Complex. Ab Initio Calculations and Fourier Transform Infrared Spectroscopy from Neon Matrix and a New Supersonic Jet Experiment Coupled to the In...

ARTICLE in THE JOURNAL OF PHYSICAL CHEMISTRY A · MARCH 2011

Impact Factor: 2.69 · DOI: 10.1021/jp111507z · Source: PubMed

CITATIONS

14

READS

124

12 AUTHORS, INCLUDING:



Pierre Asselin

Pierre and Marie Curie University - Paris 6

40 PUBLICATIONS 382 CITATIONS

SEE PROFILE



M. Esmail Alikhani

Pierre and Marie Curie University - Paris 6

107 PUBLICATIONS 1,264 CITATIONS

SEE PROFILE



Audrey Moudens

Université de Cergy-Pontoise

35 PUBLICATIONS 195 CITATIONS

SEE PROFILE



Olivier Pirali

SOLEIL synchrotron

110 PUBLICATIONS 578 CITATIONS

SEE PROFILE

The (CH₂)₂O–H₂O Hydrogen Bonded Complex. Ab Initio Calculations and Fourier Transform Infrared Spectroscopy from Neon Matrix and a New Supersonic Jet Experiment Coupled to the Infrared AILES Beamline of Synchrotron SOLEIL

M. Cirtog, P. Asselin,* P. Soulard, B. Tremblay, B. Madebène, and M. E. Alikhani

UPMC Univ Paris 06, UMR 7075, Laboratoire de Dynamique, Interactions et Réactivité (LADIR), F-75005, Paris, France

CNRS, UMR 7075, Laboratoire de Dynamique, Interactions et Réactivité (LADIR), F-75005, Paris, France

R. Georges and A. Moudens

Institut de Physique de Rennes, UMR 6251, Campus de Beaulieu, Bat 11C, Université de Rennes 1-CNRS, 35042 Rennes Cedex, France

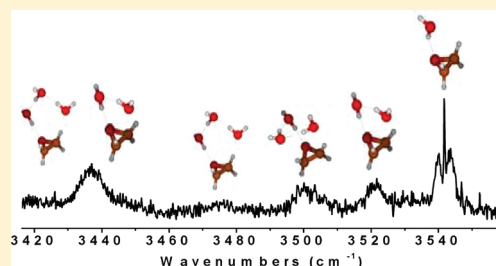
M. Goubet and T. R. Huet

Laboratoire de Physique des Lasers, Atomes et Molécules, Bâtiment P5, UMR8523 Université Lille 1-CNRS, F-59655 Villeneuve d'Ascq Cedex, France

O. Pirali[†] and P. Roy

Ligne AILES- Synchrotron SOLEIL, L'Orme des Merisiers, F-91192 Gif-sur-Yvette Cedex, France.

ABSTRACT: A series of hydrogen bonded complexes involving oxirane and water molecules have been studied. In this paper we report on the vibrational study of the oxirane–water complex (CH₂)₂O–H₂O. Neon matrix experiments and ab initio anharmonic vibrational calculations have been performed, providing a consistent set of vibrational frequencies and anharmonic coupling constants. The implementation of a new large flow supersonic jet coupled to the Bruker IFS 125 HR spectrometer at the infrared AILES beamline of the French synchrotron SOLEIL (Jet-AILES) enabled us to record first jet-cooled Fourier transform infrared spectra of oxirane–water complexes at different resolutions down to 0.2 cm^{−1}. Rovibrational parameters and a lower bound of the predissociation lifetime of 25 ps for the $\nu(\text{OH})_b = 1$ state have been derived from the rovibrational analysis of the $\nu(\text{OH})_b$ band contour recorded at respective rotational temperatures of 12 K (Jet-AILES) and 35 K (LADIR jet).



I. INTRODUCTION

A better comprehension of vibrational dynamics within hydrogen bonded complexes is relevant for atmosphere science, studies of complex liquids, and proton transfer reactions.^{1–3} In the last 20 years the development of high-resolution absorption near-infrared laser and Fourier transform techniques coupled to supersonic jets of binary mixtures seeded in rare gases has opened the way for the study of intermolecular interactions involving HX (X = F, Cl, O, ...) proton donors. The observation of intramolecular (ν_{intra}) and intermolecular (ν_{inter}) degrees of freedom has permitted, for small homo- and heterodimers^{4–17} the building of accurate ab initio intermolecular potential energy surfaces which take into account all internal coordinates^{18–20} and in turn the understanding of various state resolved dynamic processes.^{21–24}

Infrared studies involving larger hydrogen bonded complexes with stronger binding energies ($D_e = 20\text{--}40$ kJ/mol) are less

common, mainly because of the combination of homogeneous broadening effects due to predissociation dynamics and intramolecular vibration redistribution (IVR) and inhomogeneous hot band contribution related to low-frequency intermolecular modes.

For several years the LADIR group investigated medium strength hydrogen bonded one-to-one complexes between organic bases and HX hydracids by combining axisymmetric supersonic free jet (designated hereafter by LADIR jet) and cooled cell devices to absorption FTIR techniques.^{25–30} Rovibrational and dynamic parameters were derived from the rovibrational analysis of multitemperature FTIR spectra and anharmonic ab initio calculations. The observation of hot band

Received: December 3, 2010

Revised: January 20, 2011

Published: March 07, 2011

sequences in congested cell FTIR spectra showed significant anharmonic couplings between the high-frequency HX donor stretch and several low-frequency hydrogen bond modes. However such spectral analyses require a delicate deconvolution of both line broadening effects likely to question the reliability of intermolecular data.

Direct spectroscopic probes of the intermolecular potential of weakly bound homo- and heterodimers could bring more specific information because pure intermolecular transitions are expected to be only weakly broadened by fast vibrational dynamics. Owing to the limited tunability of laser sources or the poor brightness of thermal laboratory sources, only a few far-infrared (FIR) studies have been reported until now.^{31–40} Saykally's group built precise intermolecular potentials from vibration–rotation tunneling (VRT) laser spectroscopy below 100 cm^{−1} about 2-D (Ar–HCl, Ar–HF)^{33,34} and 3-D (Ar–H₂O)³⁵ prototype systems. More recently, Nelandar et al.^{36,37} measured rotationally resolved cell–Fourier transform absorption spectra of intermolecular transitions of small weakly bound dimers using FIR synchrotron radiation. Rovibrational analyses concluded that the hydrogen bond is significantly destabilized upon excitation of intermolecular HX libration modes. Lastly, combining direct FTIR absorption and Raman scattering techniques in the FIR range with supersonic expansions, Suhm et al.^{38–40} provided reliable dynamic information about intermolecular vibrations of several different sized hydrogen-bonded clusters.

For this purpose, the present work also focuses on the implementation of a large flow supersonic jet facility on the AILES beamline of the third generation synchrotron radiation (SR) source SOLEIL.⁴¹ It is developed by a consortium involving three laboratories (IPR, LADIR, and PhLAM), and it will be hereafter designated by the Jet-AILES acronym. Jet-AILES is equipped with a FTIR spectrometer, Bruker IFS 125HR (apodized maximal resolution, 0.0007 cm^{−1}). With respect to the LADIR jet, Jet-AILES takes advantage of the high radiance of the SR in the FIR range. In addition, the SR is characterized by a size diameter smaller than conventional infrared sources and therefore well adapted for probing planar jet expansions issued from narrow slit nozzles. Finally, Jet-AILES provides a larger column density of complexes whose sizes can be controlled by tuning the backing pressure.⁴²

In what follows we report on the combined experimental–theoretical study of oxirane–water molecular complexes in two separate papers. The complexes were formed in solid neon matrix and also by expanding a binary mixture of oxirane and water in argon using either the Jet-AILES facility or the LADIR jet. The present work is devoted to the oxirane–H₂O complex for which no experimental study was reported apart from a microwave one of Caminati et al.⁴³ supported by ab initio calculations. The rationale for selecting oxirane is as follows: (i) It is the simplest of ethers, largely studied by our group with HF as proton donor.^{27,30} No tunneling of H₂O (like in the case of HF^{44,45}) between the lone pairs of the ether oxygen is expected due to the rigidity of the cyclic ring which simplifies the theoretical treatment. (ii) A longer term objective for this new broad band spectroscopic probe is to characterize intermolecular vibrations of weakly bound complexes bearing H₂O as proton donor. It is therefore justified to start with a hydrated 1:1 complex of relatively high binding energy, which will be used as a first target to optimize the experimental parameters of Jet-AILES.

A subsequent paper will treat in detail the computational methods used for the assignment of larger complexes of the type (CH₂)₂O–(H₂O)_{*n*} (*n* > 1), observed both in the planar expansion of Jet-AILES and in neon matrix.

The present study is structured as follows: section II provides experimental details, namely, about the new Jet-AILES apparatus. Section III reports on neon matrix and anharmonic ab initio vibrational results. These results are completed by rovibrational data obtained from the OH proton donor stretching band ($\nu(\text{OH})_{\text{b}}$) of the (CH₂)₂O–H₂O complex formed in the jet experiments. In section IV, experimental data about vibrational and dynamic parameters of (CH₂)₂O–H₂O are then analyzed, in the light of previous results obtained on hydrogen bonded complexes bearing HF. A full set of vibrational parameters including gas phase, neon matrix, and ab initio data is finally used to estimate the equilibrium constant of the hydrated complex. A first balance sheet of the actual performances of the Jet-AILES apparatus is also presented.

II. EXPERIMENTAL AND COMPUTATIONAL DETAILS

II. 1. Helium Cryostat Device. (CH₂)₂O + H₂O samples were prepared in a closed-cycle helium cryostat (Cryomech PT-405) by slow deposition (5 mmol/h) of about 30 min in double injection (oxirane/neon and water/neon) on one side of a highly polished, Rh-plated copper mirror maintained at 3.5 K. The temperature was measured using silicon diodes, and thermal annealing was regulated by a Neocera LTC-II temperature controller.

Molar ratios (X/Ne, X = (CH₂)₂O, H₂O) ranged from 0.02 to 1%, but variable desorption of water from the stainless steel vacuum line precluded accurate concentration measurements for H₂O/Ne. Ne gas was obtained from Air Liquide with a purity of 99.995% and (CH₂)₂O was obtained from Sigma Aldrich with a purity of 99.9% while natural water was degassed in a vacuum line.

Absorption spectra in the MIR and FIR ranges were collected on samples through ICs and polyethylene windows respectively mounted on a rotatable flange separating the interferometer vacuum (10^{−3} mbar) from that of the cryostatic cell (10^{−7} mbar). Bare mirror backgrounds, recorded from 50 to 7000 cm^{−1} prior to sample deposition were used as references in processing the sample spectra. Infrared absorption spectra of the resulting samples were recorded at 3.5 K, or after sample annealing up to 12 K, in the same spectral range with a Bruker IFS 120 HR spectrometer equipped with suitable combinations of infrared sources (globar, W filament), beamsplitters (composite, KBr/Ge, Si/CaF₂), and detectors (InSb, HgCdTe, Si–B bolometer). Matrix spectra of 100–500 coadded interferograms were recorded at resolutions fixed to 0.5 cm^{−1} for high frequencies and 1 cm^{−1} for the low ones.

II. 2. LADIR Supersonic Jet. The LADIR supersonic jet-FTIR setup has already been described in detail in previous studies.²⁵ Briefly, a mixture of oxirane/Ar was bubbled in a H₂O glass container and then injected into the expansion chamber through a circular nozzle of 0.5 mm diameter. The complexes were then probed in a 16-pass multireflection arrangement by the IR beam of the LADIR high-resolution interferometer and focused on an InSb detector equipped with a band-pass filter centered at 3450 cm^{−1} and 400 cm^{−1} full width half-maximum (FWHM) to investigate the OH proton donor stretching band of (CH₂)₂O–H₂O. Each jet spectrum was the Fourier transform of ca. 1200, 2400, and 3600 coadded interferograms recorded at 1, 0.5, and at

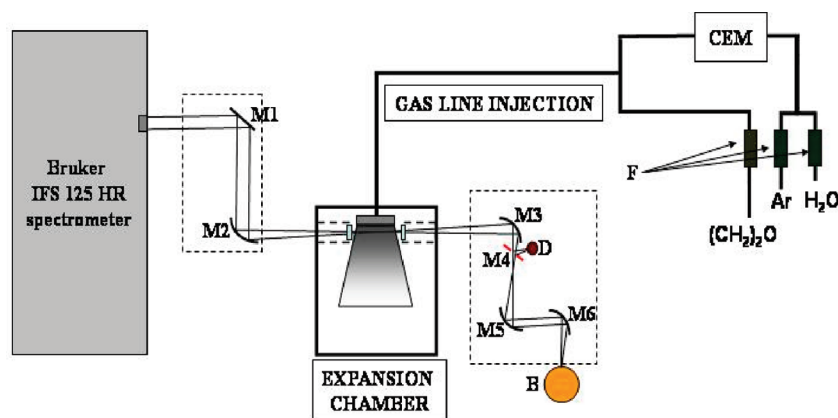


Figure 1. Schematic view of the high flow supersonic jet apparatus (Jet-AILES) in optical single pass configuration (SPC): M1, M4, plane mirrors; M2, M3, toroidal mirrors; M5, M6, off-axis parabolic mirrors; F, flowmeters, D, InSb detector; B, Si bolometer; CEM, controlled evaporation and mixing system.

0.2 cm^{-1} resolution, respectively. Oxirane from Sigma Aldrich (99.5% purity) was used without further purification.

II. 3. Jet-AILES Apparatus. An overall view of the Jet-AILES apparatus is presented in Figure 1. The continuous supersonic expansion takes place in a 400 mm diameter chamber directly evacuated by a combination of two Roots blowers (Edwards EH 500 and 2600) backed by a dry primary pump (Edwards GV 80 Drystar) leading to an effective pumping capacity of $2000\text{ m}^3/\text{h}$. The mechanical vibrations are efficiently damped by decoupling the pumping unit from the chamber thanks to two dedicated bellows mounted on the pumping line. In addition, the roots pumps are mounted on a concrete block and the chamber is rigidly fixed to the ground.

A large domain of backing pressures, which partly govern the formation of molecular complexes in an isentropic expansion, can be covered by using two slit nozzles of different lengths. For a given throughput of gas, the stagnation pressure can be adjusted by changing the width of the slit aperture between 15 and $100\text{ }\mu\text{m}$, typically. Such a fine-tuning provides an efficient mean to control and to optimize the average size and the number of molecular complexes formed in the jet expansion. Both slit nozzles are heatable up to 470 K to prevent the condensation of samples, initially liquid or solid in STP conditions. In the present study, temperature was set to 310 K to avoid the water vapor condensation. Actually, each slit nozzle is made of tempered aluminum and fixed on a stainless steel support whose temperature is regulated by two heated cartridges. A first slit nozzle of 60 mm in length is used for reaching moderate stagnation pressures (ca. 700 mbar), in a single absorption pass configuration (SPC).

A second slit nozzle of 30 mm in length can be used for higher stagnation pressures (ca. > 1.5 bar), in a multiple passes configuration (MPC) based on the optical design proposed by Gross et al.⁴⁶ This optical device has already been successfully used to probe supersonic expansions using FTIR absorption spectroscopy.^{47,48} It consists of two spherical mirrors (40 mm in diameter, $f = 25\text{ mm}$), provided with a 3 mm diameter central hole and forming a cavity of length L close to $4f$.⁴⁹

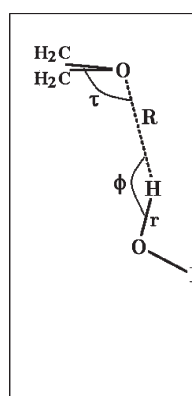
The parallel IR beam issued from the Bruker IFS 125 HR spectrometer is directed and focused into the vacuum chamber by a combination of planar (M1) and toroidal (M2, $f = 477\text{ mm}$) mirrors. Both mirrors are installed in a transfer optics compartment directly connected to the evacuated spectrometer. The IR

beam enters the expansion chamber with an optimal angle estimated to 6° (ref 49) and is coupled either to the axis center of the slit nozzle (SPC) or to the “ $L \rightarrow 4f$ ” cavity (MPC), centered on the slit axis and perpendicular to it, through the central hole of the first on-axis spherical mirror. After several reflections in the MPC, the beam is refocused at the exit hole of the second mirror and leaves the expansion chamber. The number of reflections can be varied by modifying the length of the cavity. The IR beam is finally focused in the detection chamber by a toroidal mirror (M3) and either directed on an InSb detector with a planar mirror (M4) or sent on a Si bolometer with a combination of two off-axis parabolic mirrors (M5 and M6). The InSb detector is equipped with the same band pass filter. The Si bolometer is operated at 4.2 K and equipped with diamond absorber and far-infrared cooled blocking filters (100 and 600 cm^{-1} cut-on). Both the “detection” and “transfer optics” compartments are evacuated at 10^{-4} mbar using a turbomolecular pumping unit. Two tubes equipped with wedged optical windows are set as close as possible from both sides of the expanding flow to limit the absorption of the IR beam by the residual warm gas filling the experimental chamber (Figure 1).

The IR beam is set relatively close to the nozzle exit (3–5 mm) to take advantage of the high density of the planar jet at the beginning of the expansion. The location of the shock wave forming downstream of the cold supersonic silence zone is deduced from the ratio between backing (P_0) and chamber (P_{ch}) pressures. For an expansion of argon produced by the 60 mm long, $20\text{ }\mu\text{m}$ width slit nozzle, the shock wave is estimated to be at about 40 mm downstream from the nozzle exit, far enough to not interfere with the IR beam.

Two combinations of light sources, optical configurations, beamsplitters, and detectors have been used for infrared experiments: (i) global lamp/SPC/KBr/InSb in the MIR range and (ii) SR/MPC/Mylar/Si bolometer in the FIR range.

The water vapor flow through the nozzle is regulated by a controlled evaporation and mixing system (CEM) supplied by mass regulated flows of argon gas and distilled liquid water. Oxirane gas is independently regulated by a mass flow controller. The argon/water/oxirane gas mixture flows through a heated gas line, up to the stagnation reservoir of the slit nozzle equipped with a heatable Baratron pressure gauge. The observed spectra are the Fourier transform of ca. 1600, 1200, and 1800 coadded

Table 1. The Structural, Energetic Data, and Bonded OH Frequency Shift of the Oxirane–Water Complex (C_s Group)^a


	L-I	L-II	L-III	L-IV	L-V	L-VI	Exp.
R (Å)	1.913 (1.976)	1.885 (1.949)	1.927	1.901	1.903 (1.953)	1.892	1.92±0.01
r	0.968	0.972	0.968	0.971	0.969	0.971	
τ (deg)	107	102	108	103	102	102	103±1
φ (deg)	152	153(154)	151	153	152	152	163±2
D_e	29.0	28.5	28.5	28.2	30.3	28.7	
D_e^{CP}	21.6	25.6	21.0	25.4	27.3	27.6	
D_0	20.7	21.3	21.5	21.5	21.7	20.5	
D_0^{CP}	12.3	18.1	14.0	18.7	18.7	19.4	
$\omega(\nu)$	3745[3580]	3648[3496]	3758	3673	3681[3508]	3644	3541.7
$\Delta\omega(\Delta\nu)$	140[127]	174[159]	108	138	163[160]	167	115.3

^a The vibrational averaged values are reported in parentheses. Microwave experimental data are from ref 43 [Caminati et al.]. Binding energy is in kJ/mol, and the vibrational frequencies are in cm^{-1} . Harmonic frequencies are denoted by ω , and the anharmonic ones are denoted by ν and are reported in brackets. The corresponding frequency shifts are respectively labeled as $\Delta\omega$ ($\Delta\nu$).

interferograms recorded at 1, 0.5, and at 0.2 cm^{-1} resolution, respectively.

II. 4. Computational Details. The structural, energetic, and vibrational studies of the 1:1 oxirane–water complex have been performed at three levels of theory: (1) the second order of perturbation theory (MP2), (2) the empirical dispersion corrected variant of the semiempirical hybrid density functional with perturbative second-order correlation (B2PLYPD) recently suggested by Grimme,⁵⁰ and (3) the coupled cluster method with both single and double substitutions including triple excitations noniteratively (CCSD(T)). Calculations were carried out using Gaussian09⁵¹ (for MP2 and B2PLYPD) and Molpro2008⁵² (for CCSD(T)) quantum chemical packages. Three types of basis sets have been used: two basis sets by Pople of triple- ζ quality,⁵³ namely, 6-311++G(d,p) and 6-311++G(2d,2p), and a correlation-consistent basis set developed by Dunning⁵⁴ and co-workers (Aug-cc-pVTZ).

Optimizations were obtained with “tight” convergence criteria followed by harmonic frequency calculations. The anharmonic vibrational frequencies have been calculated within the second-order vibrational perturbation theory (VPT2) as implemented in Gaussian09 code. The VPT2 calculation is not available at the CCSD(T) level.

III. RESULTS AND DISCUSSION

III. 1. Theoretical Results. For the oxirane– H_2O complex, calculations have been done at the MP2/6-311++G(d,p) level of theory in order to complete the results of a previous publication.⁴³ Additional calculations were performed in order to study the basis set effect (MP2/Aug-cc-pVTZ) as well as the correlation effect (CCSD(T)/6-311++G(d,p) and CCSD(T)/Aug-cc-pVTZ) and also to check the reliability of a newer hybrid DFT–ab initio method (B2PLYPD/6-311++G(2d,2p) and B2PLYPD/Aug-cc-pVTZ).

The optimized structural parameters for the C_s geometry conformer and energetic results are gathered in Table 1.

The method/basis set combinations are labeled as follows: L-I for MP2/6-311++G(d,p), L-II for MP2/Aug-cc-pVTZ, L-III for CCSD(T)/6-311++G(d,p), L-IV for CCSD(T)/Aug-cc-pVTZ, L-V for B2PLYPD/6-311++G(2d,2p), and L-VI for B2PLYPD/Aug-cc-pVTZ. Binding energy (D_e) and zero-point-energy corrected binding energy (D_0) are denoted by D_e^{CP} and

D_0^{CP} when they are corrected for the basis set superposition error using the counterpoise method, respectively. The vibrational frequencies and their shifts with respect to the free water molecule are given in cm^{-1} and denoted by ω , ν , $\Delta\omega$, and $\Delta\nu$, respectively, for harmonic and anharmonic frameworks.

Inspection of the structural data from Table 1 clearly indicates that the bond lengths and bond angles obtained with the six theoretical method/basis set combinations are close to each other and in a good agreement with the available experimental data. However, we underscore three points:

- The deviation angle from linearity (ϕ) varies neither with basis set nor with the theoretical method. Its calculated value is always about 10° lower than the experimental one, whatever the level of calculations.
- The directionality angle (τ) approximates more the experimental value when the basis set size increases.
- One readily note that for the three methods the intermolecular distance (R) decreases when the basis set size increases leading to a theoretical value smaller than the experimental one. Nevertheless, a better agreement is obtained between theoretical and experimental values when we consider the vibrational averaged value.

As expected, the basis set superposition error decreases when using a larger basis set. Considering the binding energy corrected for both zero-point-energy and basis set superposition error at the CCSD(T)/Aug-cc-pVTZ level ($18-19 \text{ kJ/mol}$) as the best estimation in this work, we note that only the MP2/Aug-cc-pVTZ reasonably reproduces this energy.

Finally, in order to guide assignments of our experimental vibrational bands, recorded in neon matrix and molecular jet experiments, we carried out the vibration analysis within the harmonic framework followed by anharmonic calculations using VPT2 approximation with both MP2 and B2PLYPD methods. As summarized in Table 1, the experimentally observed frequency shift for the bonded OH vibration with respect to the free H_2O is equal to 115.3 cm^{-1} . It is well-known that first, the frequency shift calculated within harmonic approximation is greater than the experimental value, and second, the corrected frequency shift for the anharmonicity effect is often independent of the size of the basis set. A quick glance on the calculated shift reported in Table 1 ($\Delta\omega$ for the harmonic value and $\Delta\nu$ for the anharmonic shift) shows that only two out of five methods used here give a result close to the experimental data obtained in the

Table 2. Vibrational Frequencies and Coupling Constants (cm^{-1}) of the $(\text{CH}_2)_2\text{O}-\text{H}_2\text{O}$ Complex^a

fundamentals	experimental		calculated	calculated anharmonic coupling constants		
	gas	matrix	anharmonic L-I; L-II; L-V	δ	$\nu(\text{OH})_{\text{b}}$	$\nu(\text{OH})_{\text{f}}$
ν_{dinp}			45 (1); 74; 85	2	4	0
ν_{doup}			54 (11); 3; 254	4	3	0
ν_{T}			88 (56); 34; 430	10	-1	-3
ν_{O}		[182.7] (10)	171 (8); 180; 190	-2	6	3
ν_{linp}		[335.5] (50)	335 (59); 330; 372	-16	35	-4; -2; 1 [3.1]
ν_{loup}		[520.6] (25)	533 (31); 535; 482	7; 6; 7 [5.3]	51	2
δ		[1605.3] (20)	1600 (24); 1591; 1617	-19; -20; -24 [-14]	-18; -7; -8 [-10.4]	-19
$\nu(\text{OH})_{\text{b}}$	3541.7	[3535.8] (100)	3580 (100); 3496; 3508		-91; -98; -101 [-106.8]	-55
$\nu(\text{OH})_{\text{f}}$		[3718.2] (50)	3784 (38); 3739; 3759			-73
Combination Modes						
$\delta + \nu_{\text{loup}}$		[2131.2]	2094; 2132; 2130			
$\nu(\text{OH})_{\text{f}} + \nu_{\text{linp}}$		[4054.7]	4115; 4066; 4132			
$\nu(\text{OH})_{\text{b}} + \delta$		[5130.6]	5161; 5079; 5117			
Two-Quanta Modes						
2δ		[3182]	3161; 3141; 3185			
$2\nu(\text{OH})_{\text{b}}$		[6858]	6978; 6749; 6816			

^aTheoretical results have been computed at the MP2/6-311++G(d,p) (L-I), MP2/Aug-cc-pVTZ (L-II), and B2PLYPD/6-311++G(2d,2p) (L-V) levels, respectively. Matrix experimental data are reported in brackets and relative intensities in parentheses.

supersonic jet experiment. By accepting the CCSD(T)/Aug-cc-pVTZ harmonic shift value (138 cm^{-1}) as a reference, one sees that the two other methods (MP2/Aug-cc-pVTZ and B2PLYPD/6-311++G(2d,2p)) overestimate this shift by around 20% while CCSD(T)/6-311++G(d,p) underestimates it by 14%. Consequently, thanks to the good quality of the vibrational analysis of the MP2/6-311++G(d,p), the availability of the anharmonic correction and also its computational low cost, we chose this technique to help the study of infrared experimental spectra. Nevertheless, we should emphasize that this method is not the best one to provide a good description of other properties (geometrical, energetic and electronic ones). For this reason and also for the sake of comparison, we report a number of vibrational data obtained by the methods MP2/Aug-cc-pVTZ and B2PLYPD/6-311++G(2d,2p) in Table 2.

The effects of theoretical methods including a large number of recently developed DFT functionals for noncovalent systems will be presented in detail in a forthcoming paper applied to the study of $(\text{CH}_2)_2\text{O}-(\text{H}_2\text{O})_n$ complexes where $n = 1, 2$, and 3.

III. 2. Neon Matrix Data. The high detectivity of the neon matrix isolation technique is likely to reveal the presence of a few intense modes belonging to the $(\text{CH}_2)_2\text{O}-\text{H}_2\text{O}$ complex such as fundamentals (intra- and intermolecular ones), combinations, and overtones. Due to the small neon matrix induced perturbations, the observed vibrational frequencies are expected to be slightly shifted with respect to gas phase ones.^{55,56}

When $(\text{CH}_2)_2\text{O}$ and H_2O are codeposited in a neon matrix, new strong bands appear in the vicinity of H_2O fundamentals and in the region of intermolecular modes. Figure 2 displays a series of neon matrix spectra recorded in the OH stretching mode region of H_2O for different molar ratios (a) to (f) of the $(\text{CH}_2)_2\text{O}/\text{H}_2\text{O}/\text{Ne}$ ternary mixture. In addition to the $(\text{H}_2\text{O})_2$ band⁵⁷ at 3590.5 cm^{-1} , two absorptions at 3535.8 and 3501 cm^{-1} are observed. The concentration dependence of the band at 3535.8 cm^{-1} over a very wide range presents the same linear dependence with respect to either H_2O or $(\text{CH}_2)_2\text{O}$,

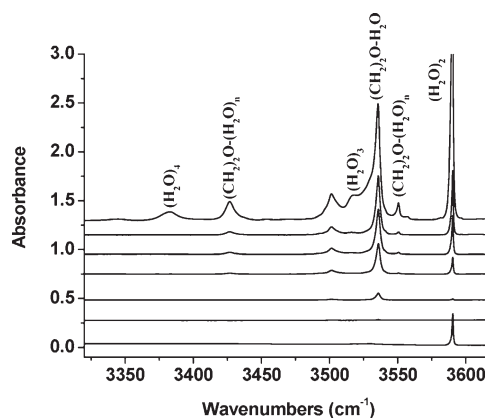


Figure 2. Neon matrix spectra after deposition at 3.5 K recorded in the O–H symmetric stretching region of H_2O and of the $(\text{CH}_2)_2\text{O}-\text{H}_2\text{O}$ complex for different dilutions of the ternary mixture $(\text{CH}_2)_2\text{O}/\text{H}_2\text{O}/\text{Ne}$: (a) $\text{H}_2\text{O}/\text{Ne} = 1/1000$, (b) $(\text{CH}_2)_2\text{O}/\text{Ne} = 1/1000$, (c) $(\text{CH}_2)_2\text{O}/\text{H}_2\text{O}/\text{Ne} = 1/0.2/1000$, (d) $1/0.5/1000$, (e) $1/1/1000$, (f) $1/3/1000$, (g) $1/10/1000$.

which gives confidence for assigning this absorption to the $\nu(\text{OH})_{\text{b}}$ band of the $(\text{CH}_2)_2\text{O}-\text{H}_2\text{O}$ complex. Since the band intensity at 3501 cm^{-1} has a high dependence in oxirane but not a clear dependence in H_2O , this absorption could not be ascribed to any specific complex and is noted by $((\text{CH}_2)_2\text{O})_n(\text{H}_2\text{O})_m$.

When H_2O concentration is growing, four bands at 3550.6 , 3529.6 , 3426.8 , and 3382.0 cm^{-1} appear in the same region (Figure 2g) with a faster intensity increase than that of the $\nu(\text{OH})_{\text{b}}$ complex band. Two of them, at 3529.6 and 3382.0 cm^{-1} , have been assigned to water aggregates $((\text{H}_2\text{O})_3$ and $(\text{H}_2\text{O})_4$, respectively),⁵⁸ and the two others to oxirane–water species containing more than one H_2O molecule. These bands will be analyzed in a subsequent paper.

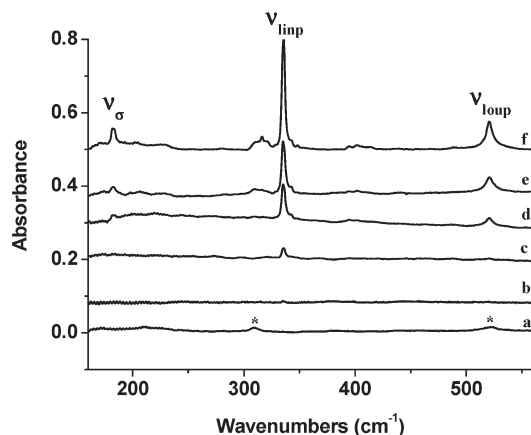


Figure 3. Neon matrix spectra after deposition at 3.5 K in the intermolecular region of $(\text{CH}_2)_2\text{O}-\text{H}_2\text{O}$ complex for different dilutions of the ternary mixture $(\text{CH}_2)_2\text{O}/\text{H}_2\text{O}/\text{Ne}$: (a) $\text{H}_2\text{O}/\text{Ne} = 1/1000$, (b) $(\text{CH}_2)_2\text{O}/\text{Ne} = 1/1000$, (c) $(\text{CH}_2)_2\text{O}/\text{H}_2\text{O}/\text{Ne} = 1/0.2/1000$, (d) $1/0.5/1000$, (e) $1/1/1000$, (f) $1/3/1000$. Bands marked by an asterisk designate intermolecular bands of $(\text{H}_2\text{O})_2$.

Accompanying the absorption at 3535.8 cm^{-1} in the $\nu(\text{OH})_b$ stretching region, other absorptions in the far-, mid-, and near-infrared regions can be correlated with this band and exhibit the same linear dependence with respect to either H_2O or $(\text{CH}_2)_2\text{O}$ concentration. This proves that all these absorptions belong to species with the same 1:1 stoichiometry.

More specifically, in the region of the absorptions related to ν_1 and ν_3 bands of H_2O monomer, a new band is observed at 3718.2 cm^{-1} . On the grounds of calculated vibrational frequencies and relative intensities with respect to $\nu(\text{OH})_b$, this band is assigned to the OH free stretching mode ($\nu(\text{OH})_f$) of the complex. In the ν_2 region of the H_2O monomer, a weak band at 1605.3 cm^{-1} , six times weaker than the $\nu(\text{OH})_b$ band, could be observed. With the same arguments it is assigned to the $\delta(\text{H}-\text{O}-\text{H})$ bending mode of the complex.

There is no band below 600 cm^{-1} for the oxirane monomer. Accordingly, three bands observed at 182.7 , 335.5 , and 520.6 cm^{-1} (Figure 3) with relative intensities of 0.1 , 0.5 , and 0.25 , respectively, correspond to intermolecular vibrations in the complex. With the help of ab initio calculations, these bands are unambiguously assigned to intermolecular stretching (ν_σ), in plane libration (ν_{linp}) and out of plane libration (ν_{loup}) modes calculated at 171 , 335 , and 533 cm^{-1} with relative intensities of 0.1 , 0.66 , and 0.33 (Table 2).

Finally, five additional weaker absorptions are observed at 2131.2 , 3182 , 4054.7 , 5130.6 , and 6858 cm^{-1} . These bands should proceed from combinations, of the type $(\nu_{\text{intra}} + \nu_{\text{inter}})$ and $(\nu_{\text{intra}} + \nu_{\text{intra}})$, or to overtone ($2\nu_{\text{intra}}$). The difference between the 2131.2 cm^{-1} band and the δ band is 525.9 cm^{-1} , very close to the ν_{loup} mode observed at 520.6 cm^{-1} justifies to assign it to the $(\delta + \nu_{\text{loup}})$ combination with an anharmonicity coupling constant $x_{\delta\text{loup}}$ of 5.3 cm^{-1} . Notice that the ab initio calculations predict the $(\delta + \nu_{\text{loup}})$ combination band to 2094 cm^{-1} and $x_{\delta\text{loup}}$ to 6.6 cm^{-1} (Table 2), in line with our assignment. In the same manner, we assign the bands at 3182 , 4054.7 , 5130.6 , and 6858 cm^{-1} to the 2δ , $\nu(\text{OH})_f + \nu_{\text{linp}}$, $\nu(\text{OH})_b + \delta$, $2\nu(\text{OH})_b$ bands (Table 2).

III. 3. Jet-Cooled Data. *III. 3a. Jet-FTIR Spectra.* The strongest band of the $(\text{CH}_2)_2\text{O}-\text{H}_2\text{O}$ complex, the $\nu(\text{OH})_b$ band, has

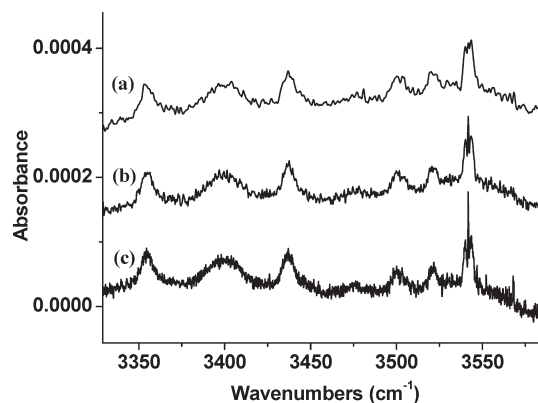


Figure 4. Jet-AILES FTIR spectrum in the $\nu(\text{OH})_b$ stretching region of $(\text{CH}_2)_2\text{O}-\text{H}_2\text{O}$ at respective resolutions of (a) 1 cm^{-1} , (b) 0.5 cm^{-1} , and (c) 0.2 cm^{-1} .

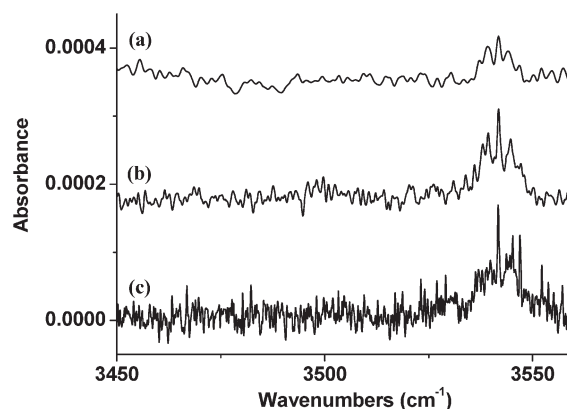


Figure 5. LADIR jet FTIR spectrum in the $\nu(\text{OH})_b$ stretching region of $(\text{CH}_2)_2\text{O}-\text{H}_2\text{O}$ at respective resolutions of (a) 1 cm^{-1} , (b) 0.5 cm^{-1} , and (c) 0.2 cm^{-1} .

been observed for the first time in the gas phase in both supersonic expansions.

Two series of jet spectra recorded at different resolutions in the $\nu(\text{OH})_b$ region of $(\text{CH}_2)_2\text{O}-\text{H}_2\text{O}$ are shown in Figure 4 (Jet-AILES) and Figure 5 (LADIR jet). For both molecular beam expansions the conditions of dilution and reservoir pressure P_0 of the ternary mixture $(\text{CH}_2)_2\text{O}/\text{H}_2\text{O}/\text{Ar}$ are adjusted to enhance formation of the $(\text{CH}_2)_2\text{O}-\text{H}_2\text{O}$ dimer with respect to larger complexes. The conditions of dilution are somewhat different depending on the two devices: for Jet-AILES, $(\text{CH}_2)_2\text{O}/\text{H}_2\text{O}/\text{Ar} = 1/1.5/75$ with a $(\text{CH}_2)_2\text{O}$ flow fixed to 0.1 slm , $P_0 = 700\text{ mbar}$ and $P_{\text{ch}} = 0.1\text{ mbar}$; for the LADIR jet $(\text{CH}_2)_2\text{O}/\text{H}_2\text{O}/\text{Ar} = 1/1/4$ $P_0 = 200\text{ mbar}$ and $P_{\text{ch}} = 0.0016\text{ mbar}$ with a $(\text{CH}_2)_2\text{O}$ flow fixed to 0.07 slm . In both jet spectra, a characteristic PQR rovibrational band contour is observed at 3541.7 cm^{-1} , more and more resolved with increasing resolution.

The observation of a unique band in the LADIR jet spectrum confirms that low values of P_0 strongly enhance the 1:1 complex formation. Consequently the band at 3541.7 cm^{-1} is assigned to the $\nu(\text{OH})_b$ mode of the $(\text{CH}_2)_2\text{O}-\text{H}_2\text{O}$ complex, 115.3 cm^{-1} red shifted with respect to the monomer.

Additional broad and unstructured absorptions are observed in the high-pressure jet spectra (Figure 4). These bands are assigned either to water polymers $(\text{H}_2\text{O})_{3-5}$ ⁴² or to higher size

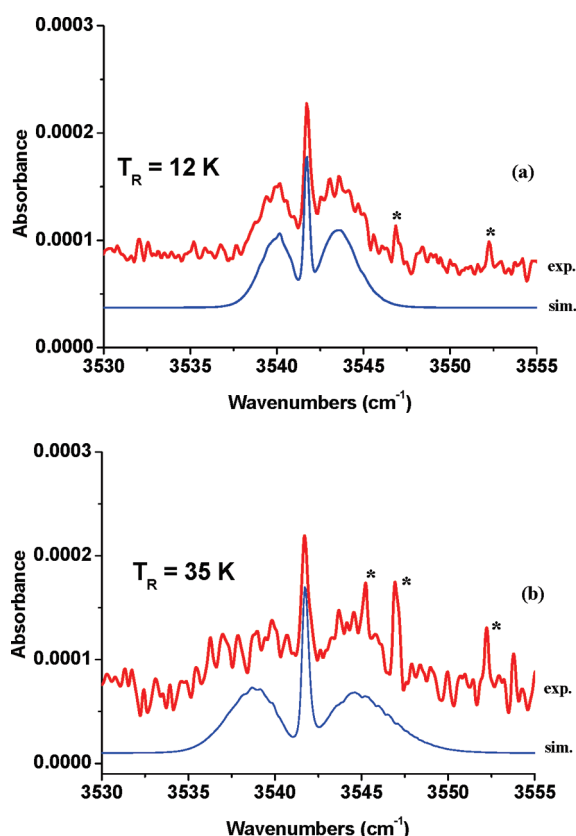


Figure 6. Comparison between FTIR experiments and simulation for (a) Jet-AILES spectra and (b) LADIR jet spectra of the $\nu(\text{OH})_{\text{b}}$ band of $(\text{CH}_2)_2\text{O}-\text{H}_2\text{O}$ at 0.2 cm^{-1} resolution. Bands marked by an asterisk correspond to ν_3 rovibrational bands of H_2O monomer.

complexes between H_2O and $(\text{CH}_2)_2\text{O}$. Their analysis will be presented elsewhere.

III. 3b. Band Contour Simulations of Jet-FTIR Spectra. Starting from the simulation of the rotational structure for an unperturbed rigid asymmetric rotor, rovibrational parameters of the $\nu(\text{OH})_{\text{b}}$ band at different jet temperatures could be derived. Several parameters are initially fixed: (i) the ground-state rotational constants obtained from microwave experiments;⁴³ (ii) the band hybridization computed from the projection of the dipole moment related at the normal coordinate onto the molecular inertial axes; (iii) the instrumental resolution $\Delta\nu_{\text{fwhm}}$ and the shape of the response function (Happ-Genzel in this case).

Adjustable molecular parameters of the simulation are the rovibrational coupling constants $\alpha(\text{OH})_{\text{b}}^X$ with $X = A, B, C$ (rotational constants), the rotational temperature T_{R} , the band center frequency $\nu(\text{OH})_{\text{b}}$, and the effective line width γ . Our best fit to reproduce the band contours at 0.2 cm^{-1} resolution is displayed in Figure 6 with Jet-AILES (a) and LADIR jet (b) expansions. Fitting parameters are $\alpha(\text{OH})_{\text{b}}^A$ and $(\alpha(\text{OH})_{\text{b}}^B + \alpha(\text{OH})_{\text{b}}^C)$ coupling constants, equal to $-0.0015(5)$ and $-0.002(1)\text{ cm}^{-1}$, respectively, the band center frequency $\nu(\text{OH})_{\text{b}}$ equal to $3541.7(1)\text{ cm}^{-1}$ and the line width γ equal to 0.2 cm^{-1} .

The reliability of the molecular parameter set for both jet spectra is proved by the good agreement obtained between experimental and simulated spectra at different temperatures. As the value derived for the effective line width is about equal

to $\Delta\nu_{\text{FWHM}}$, we can only specify a superior limit for γ and consequently a lower bound for the predissociation lifetime (25 ps).

III. 4. Discussion. Detectivity performances of the Jet-AILES apparatus have been examined in the middle infrared (MIR) region with a Globar source, using the $(\text{CH}_2)_2\text{O}-\text{H}_2\text{O}$ hydrogen bonded complex results.

In the MIR region, a signal-to-noise ratio (S/N) of 30 is obtained for the $\nu(\text{OH})_{\text{b}}$ band with 1800 coadded scans at 0.2 cm^{-1} resolution. Taking into account the optical path of 6 cm (SPC), our detection limit is estimated to $8 \times 10^{-6}\text{ cm}^{-1}$. When the Globar source is combined with optical MPC, a sharp drop of S/N is observed for apertures larger than 1.5 mm. In fact, important photon loss takes place when the infrared beam crosses the optical cavity through 3 mm diameter holes of the MPC. On the other hand, when the narrow spatial distribution of the SR source is combined with optical MPC, the absorption signal is multiplied by 4 and no photon loss is observed. In all, the noise level of the MPC/SR combination in the FIR region decreases by a factor 6 compared to the MPC/Globar one.

This configuration has been used for searching the most intense intermolecular mode (ν_{linp}) of the $(\text{CH}_2)_2\text{O}-\text{H}_2\text{O}$ complex, knowing that relative intensities of 0.5 and 0.6 (compared to $\nu(\text{OH})_{\text{b}}$) were obtained from matrix experiments and ab initio calculations, respectively. Considering intensity estimates of ν_{linp} and the ultimate noise level reached (1.2×10^{-4} for 500 scans at 0.5 cm^{-1} resolution) it is pointed out that S/N should be multiplied by about 2 to pass beyond the detection threshold of ν_{linp} .

Compared to the LADIR jet, two major improvements of the Jet-AILES apparatus should be underlined:

- For the same absorption relative to a 1:1 complex ($\nu(\text{OH})_{\text{b}}$ band) at equivalent resolution and number of scans, the S/N ratio is multiplied by 3. If one assumes that the effective gain in absorbance of the multipass White optics of the LADIR jet is about 8 with a bound error of $\pm 30\%$, the detectivity of Jet-AILES is estimated to be about 20 times higher, without MPC. This gain is essentially due to the large difference between pumping speeds enabling to probe higher densities of molecular complexes,
- Thanks to the larger available range of backing pressures, different sizes of complexes can be stabilized in the same supersonic planar expansion. High values of P_0 also enhance the rovibrational cooling, as proved by the low value of T_{R} (12 K) derived from the simulated Jet-AILES spectra to be compared with 35 K for the LADIR jet.

Rather different temperatures between both jet-FTIR spectra enabled refinement the $\nu(\text{OH})_{\text{b}}$ band contour analysis of $(\text{CH}_2)_2\text{O}-\text{H}_2\text{O}$ and derivation of a consistent set of rovibrational parameters (band center frequency, rovibrational coupling constants, and homogeneous line width). The variation of excited state rotational constants, between 0.3 and 0.8% for $\alpha(\text{OH})_{\text{b}}^X/X_0$, is for the most part smaller than in the case where HF acts as proton donor (for example with $(\text{CH}_2)_2\text{O}-\text{HF}$,²⁷ α_s^X/X_0 falls in the range 2–4%). This result suggests that the geometry of $(\text{CH}_2)_2\text{O}-\text{H}_2\text{O}$ remains practically unchanged upon excitation of $\nu(\text{OH})_{\text{b}}$.

The large gap between upper bound γ values (0.2 cm^{-1} compared to 3.3 cm^{-1}) when H_2O instead of HF is bonded to $(\text{CH}_2)_2\text{O}$ can be explained by important differences in the factors

entering the effective line width of these complexes:

- Earlier analyses have shown that the γ parameter contains information on the predissociation dynamics^{25,26} which is expected to be faster with H₂O as proton donor: with $D_0^{\text{CP}} = 1030 \text{ cm}^{-1}$ at the MP2/6-311++G(d,p) level, the available excess energy upon donor stretch excitation is about 2500 cm^{-1} for H₂O and only about 1000 cm^{-1} for HF.³⁰
- The vibrational density of states at the excitation energy, and therefore IVR contribution is expected to be larger with H₂O because this 1:1 complex possesses one more intermolecular vibration below 100 cm^{-1} .
- Anharmonic couplings between the intramolecular donor stretch mode ($\nu(\text{OH})_{\text{b}}$, ν_{HF}) and intermolecular modes are much smaller in the case of H₂O: from calculated anharmonic coupling constants (Table 2) of the three low frequency intermolecular $\nu_{\delta_{\text{in}}}$, $\nu_{\delta_{\text{out}}}$, and ν_{σ} modes, x_{ij}/ν_j ratios fall in the 3.2–6.5% range, while they reach 13–20% (from experimental values) for HF.²⁷

The factors (i) and (ii) are rather directed at a faster predissociation dynamics of (CH₂)₂O–H₂O but our experimental data evidence a reverse effect on γ . We conclude that the third factor, namely, the strength of anharmonic couplings x_{ij} , mainly contributes to speed up vibrational dynamics of hydrogen bonded complexes bearing a strong acid. Consequently we can only specify a lower bound on the predissociation lifetime, namely, 25 ps for the $\nu(\text{OH})_{\text{b}} = 1$ state of (CH₂)₂O–H₂O.

As expected, vibrational frequencies measured in neon matrix are a few cm^{-1} shifted with respect to the gas phase (-6 cm^{-1} for $\nu(\text{OH})_{\text{b}}$). A good agreement is observed between vibrational frequencies derived from MP2/6-311++G(d,p) calculations and neon matrix experiments with deviations typically ranged around 1(1)% except for the stretching intermolecular ν_{σ} mode which is calculated about 7% lower than the matrix value (Table 2). This result deserves some comments: it is well-established that the MP2 method overestimates the strength of the hydrogen bond provided using a large basis set; therefore one expects to calculate higher intermolecular frequencies and lower intramolecular ones. It is likely that the good match between experimental and calculated data is due to an error compensation between the MP2 method and the 6-311++G(d,p) basis set. We also note that calculated relative intensities reproduced those of the observed intermolecular modes.

Finally, from the detection of weak combination and overtone bands, five x_{ii} or x_{ij} anharmonic coupling constants could be derived. As shown in Table 2, a systematic overestimation for MP2/6-311++G(d,p) values of x_{ii} with respect to the experimental ones is observed (up to 8 cm^{-1} for $x_{\text{OH}_b\delta}$) while the diagonal term $x_{\text{OH}_b\text{OH}_b}$ is underestimated by about 15% (-91 cm^{-1} vs -106.8 cm^{-1}). For comparison, the anharmonic coupling constants derived with the same theoretical level for (H₂O)₂ are very close to the neon matrix ones,⁵⁷ which fully validates the ability to use anharmonic vibrational calculations as a support for assigning 1:1 complex fundamentals and especially combination bands.

Using equilibrium statistical thermodynamics⁵⁹ with monomers and 1:1 complex vibrational frequencies/rotational constants⁴³ and both binding energies (D_{e} and D_{e}^{CP}), the corresponding enthalpy and entropy changes upon complexation can be calculated to derive the equilibrium constant $K_{\text{p}}(T)$

Table 3. Equilibrium Constant of the Title Reaction: Oxirane + Water = 1:1 Complex.^a

			$K_{\text{p}}(298.15 \text{ K}) (\text{atm}^{-1})$	
			using D_{e}	using D_{e}^{CP}
MP2	6-311++G(d,p)	harmonic	0.016	0.0008
		anharmonic	0.112	0.006
		anharmonic+exp.	0.065	0.003
	Aug-cc-pVTZ	harmonic	0.017	0.004
		anharmonic	2.871	0.892
		anharmonic+exp.	1.798	0.558
CCSD(T)	6-311++G(d,p)	harmonic	0.013	0.0006
		Aug-cc-pVTZ	0.012	0.004
B2PLYPD	6-311++G(2d,2p)	harmonic	0.019	0.006
		anharmonic	0.0008	0.0002
		anharmonic+exp.	0.004	0.001
	Aug-cc-pVTZ	harmonic	0.019	0.012

^a “Anharmonic+exp.” indicates that a number of theoretical parameters (vibrational frequencies of monomers, part of those of the complex, and the rotational constants) were replaced by their experimental values.

of the oxirane–water complex. Three data sets of vibrational frequencies have been employed for comparison: first and second ab initio harmonic and anharmonic vibrational frequencies, and third a mixed ab initio–experimental one with neon matrix and jet frequencies. All the $K_{\text{p}}(298.15 \text{ K}) (\text{atm}^{-1})$ values are reported in Table 3.

A comparative study of the $K_{\text{p}}(298.15 \text{ K})$ values calculated with harmonic frequencies shows clearly two trends:

- First, we find almost the same value for the $K_{\text{p}}(298.15 \text{ K})$ constant using D_{e} as binding energy, whatever the method/basis set combination. $K_{\text{p}}(298.15 \text{ K})$ varies in the range 0.012–0.019.
- Second, when we use the BSSE corrected binding energy (D_{e}^{CP}) the equilibrium constant value decreases substantially with respect to its value obtained with D_{e} .
- Taking as a reference the $K_{\text{p}}(298.15 \text{ K})$ value obtained at CCSD(T)/Aug-cc-pVTZ using D_{e}^{CP} , we note that the MP2/Aug-cc-pVTZ gives a similar result, while the B2PLYPD/Aug-cc-pVTZ overestimates the $K_{\text{p}}(298.15 \text{ K})$ value by a factor 3.

As shown in Table 3, the $K_{\text{p}}(298.15 \text{ K})$ value calculated with the anharmonic frequencies presents an erratic behavior, essentially due to the ill-representation of the anharmonicity effect on the three lowest frequencies of the 1:1 complex (see Table 2 for bending in plane, out-of-plane, and torsion modes). This issue is particularly pronounced when we focus on the basis set effect in going from the MP2/6-311++G(d,p) to the MP2/Aug-cc-pVTZ level. Contrarily, the $K_{\text{p}}(298.15 \text{ K})$ value substantially decreases due to the anharmonicity effect at the B2PLYPD/6-311++G(2d,2p) level of theory. It is therefore difficult to draw a clear conclusion on the anharmonicity effect on the $K_{\text{p}}(298.15 \text{ K})$ value for method/basis set combination. Nevertheless, it is worth noting that with the MP2/6-311++G(d,p) level of theory giving a set of anharmonic vibrational frequencies close enough to the available experimental values, it could be confidently used as a model to calculate the equilibrium constant for the studied chemical reaction. Particularly, this calculation could be improved by replacing the calculated low intermolecular frequencies by corresponding experimental ones when available. For

instance, the $K_P(298.15\text{ K})$ value reduces twice when going from the pure ab initio anharmonic data, obtained at the MP2/6-311++G(d,p) level, to mixed ab initio–experimental data. Moreover, these values (0.006 and 0.003) are very close to that calculated at the CCSD(T)/Aug-cc-pVTZ level (0.004).

Consequently, experimental vibrational data, particularly the low intermolecular ones, should improve the accuracy of the $K_P(T)$ estimation and accordingly provide a reliable determination of densities of hydrogen bonded complexes as for example, atmospheric abundances of hydrated complexes to evaluate their role in the Earth's atmospheric chemistry and climate.^{60,61}

IV. CONCLUSION

Gas phase rovibrational data were obtained about the OH donor stretch band of $(\text{CH}_2)_2\text{O}-\text{H}_2\text{O}$ stabilized in the respective planar and axisymmetric supersonic expansions of Jet-AILES at 12 K and of the LADIR jet at 35 K. Vibrational fundamentals (three intramolecular H_2O perturbed and three intermolecular ones) and five anharmonic coupling constants have been derived from the neon matrix study which are well reproduced by anharmonic vibrational calculations.

A large flow supersonic jet has been successfully implemented on the far-infrared beamline of the synchrotron facility SOLEIL. First Fourier transform experiments in the middle infrared range using a thermal source enabled to detect in the seeded argon supersonic expansion of an oxirane–water mixture several sized hydrogen bonded complexes of the type $(\text{CH}_2)_2\text{O}-(\text{H}_2\text{O})_n$, $n \geq 1$.

Extensive efforts are currently pursued to increase the detectivity of Jet-AILES, especially to reach the FIR range, by improving the MPC settings to gain in absorbance sensitivity and also in a systematic sweep of all jet parameters (slit nozzle width, backing pressure, carrier gas, and water flows) allowing to maximize the absorption signal for every molecular system investigated.

AUTHOR INFORMATION

Corresponding Author

*Electronic mail: pierre.asselin@upmc.fr.

Notes

[†]Also at Institut des Sciences Moléculaires d'Orsay, CNRS, Bat. 210, Université Paris-Sud, 91405 Orsay, France.

ACKNOWLEDGMENT

We wish to thank J.-B. Brubach, M. Rouzières, and D. Balcon from the AILES group at SOLEIL for assistance and advice during the implementation of the high-pressure supersonic jet on the AILES-A beamline. We are grateful to SOLEIL for provision of synchrotron radiation facilities. Support from the ANR-08-BLAN-0054 contract and from the “Physico-Chimie du Milieu Interstellaire” Program is acknowledged by the Lille group. Support from the “Projet Exploratoire PluridisciplinaireS, Physique Théorique et ses Interfaces” (CNRS) is acknowledged by the Rennes and Paris groups.

REFERENCES

(1) Pimentel, G. C.; McClellan, A. C. *The Hydrogen Bond*; Freeman: San Francisco, CA, 1960.

(2) Schuster, P.; Zundel, G.; Sandorfy, C., Eds.; *The Hydrogen Bond: Recent Developments in Theory and Experiments*; North Holland: Amsterdam, 1976.

(3) Jeffrey, G. A.; Saenger, W. *Hydrogen Bonding in Biological Structures*; Springer: Berlin, 1991.

(4) Huang, Z. S.; Jucks, K. W.; Miller, R. E. *J. Chem. Phys.* **1986**, *85*, 3338.

(5) Huang, Z. S.; Miller, R. E. *J. Chem. Phys.* **1988**, *88*, 8008.

(6) Marshall, M. D.; Bohac, E. J.; Miller, R. E. *J. Chem. Phys.* **1992**, *97*, 3307.

(7) Coker, D. F.; Miller, R. E.; Watts, R. O. *J. Chem. Phys.* **1985**, *82*, 3554.

(8) Busarow, K. L.; Cohen, R. C.; Blake, G. A.; Laughlin, K. B.; Lee, Y. T.; Saykally, R. J. *J. Chem. Phys.* **1989**, *90*, 3937.

(9) Cruzan, J. D.; Viant, M. R.; Brown, M. G.; Saykally, R. J. *J. Phys. Chem.* **1997**, *101*, 9022.

(10) Elrod, M. J.; Saykally, R. J. *J. Chem. Phys.* **1995**, *103*, 921.

(11) Schuder, M. D.; Lovejoy, C. M.; Lascola, R.; Nesbitt, D. J. *J. Chem. Phys.* **1993**, *99*, 4346.

(12) Suhm, M. A.; Farrell, J. T.; Ashworth, S. H.; Nesbitt, D. J. *J. Chem. Phys.* **1993**, *98*, 5985.

(13) Quack, M.; Suhm, M. *J. Chem. Phys.* **1991**, *95*, 28.

(14) Luckhaus, D.; Quack, M.; Schmitt, U.; Suhm, M. *Ber. Bunsen-Ges. Phys. Chem.* **1995**, *99*, 457.

(15) Anderson, D. T.; Davis, S.; Nesbitt, D. J. *J. Chem. Phys.* **1996**, *104*, 6225.

(16) Quack, M.; Suhm, M. Spectroscopy and Quantum Dynamics of Hydrogen Fluoride Clusters. In *Advances in Molecular Vibrations and Collision Dynamics, Vol. III, Molecular Clusters*; Bowman, J., Bacic, Z., Eds.; JAI Press: Greenwich, CT, 1998; p 205.

(17) Hartz, C.; Wofford, B. A.; Meads, R. F.; Lucchese, R. R.; Bevan, J. W. *Rev. Sci. Instrum.* **1995**, *66* (8), 4375.

(18) Quack, M.; Suhm, M. *Mol. Phys.* **1990**, *69*, 791.

(19) Kloppe, W.; Quack, M.; Suhm, M. *Chem. Phys. Lett.* **1996**, *261*, 35.

(20) Fellers, R. S.; Braly, L. B.; Saykally, R. J.; Leforestier, C. *J. Chem. Phys.* **1999**, *110*, 6306.

(21) Dayton, D. C.; Miller, R. E. *Chem. Phys. Lett.* **1988**, *143*, 181.

(22) Nesbitt, D. J.; Lovejoy, C. M. *J. Chem. Phys.* **1992**, *96*, 5712.

(23) Jucks, K. W.; Huang, Z. S.; Miller, R. E. *J. Chem. Phys.* **1987**, *86*, 1098.

(24) Lovejoy, C. M.; Nesbitt, D. J. *J. Chem. Phys.* **1989**, *90*, 4671.

(25) Goubet, M.; Asselin, P.; Soulard, P.; Lewerenz, M.; Latajka, Z. *J. Chem. Phys.* **2004**, *121*, 7784.

(26) Asselin, P.; Goubet, M.; Lewerenz, M.; Soulard, P.; Perchard, J. P. *J. Chem. Phys.* **2004**, *121*, 5241.

(27) Asselin, P.; Goubet, M.; Latajka, Z.; Soulard, P.; Lewerenz, M. *Phys. Chem. Chem. Phys.* **2005**, *7*, 592.

(28) Asselin, P.; Soulard, P.; Madebène, B.; Alikhani, M. E.; Lewerenz, M. *Phys. Chem. Chem. Phys.* **2006**, *8*, 1785.

(29) Asselin, P.; Soulard, P.; Madebène, B.; Lewerenz, M. *Phys. Chem. Chem. Phys.* **2007**, *9*, 2868.

(30) Cirtog, M.; Asselin, P.; Soulard, P.; Madebène, B.; Alikhani, M. E. *Phys. Chem. Chem. Phys.* **2010**, *12*, 12299.

(31) von Puttkammer, K.; Quack, M. *Mol. Phys.* **1987**, *62*, 1047.

(32) Cohen, R. C.; Saykally, R. J. *J. Phys. Chem.* **1992**, *96*, 1024.

(33) Busarow, K. L.; Blake, G. A.; Laughlin, K. B.; Cohen, R. C.; Lee, Y. T.; Saykally, R. J. *J. Chem. Phys.* **1988**, *89*, 1268.

(34) Fraser, G. T.; Pine, A. S. *J. Chem. Phys.* **1986**, *85*, 2502.

(35) Cohen, R. C.; Busarow, K. L.; Laughlin, G. B.; Blake, G. A.; Havenith, M.; Lee, Y. T.; Saykally, R. J. *J. Chem. Phys.* **1988**, *89*, 4494.

(36) Wugt Larsen, R.; Hegelund, F.; Nelander, B. *Phys. Chem. Chem. Phys.* **2004**, *6*, 3077.

(37) Wugt Larsen, R.; Hegelund, F.; Nelander, B. *J. Phys. Chem. A* **2004**, *108*, 1524.

(38) Liu, Y.; Weimann, M.; Suhm, M. A. *Phys. Chem. Chem. Phys.* **2004**, *6*, 3315.

- (39) Wugt Larsen, R.; Suhm, M. A. *Phys. Chem. Chem. Phys.* **2010**, *12*, 8152.
- (40) Xue, Z.; Suhm, M. A. *J. Chem. Phys.* **2009**, *131*, 054301.
- (41) Roy, P.; Rouzières, M.; Qi, Z. M.; Chubar, O. *Infrared Phys. Technol.* **2006**, *49*, 139.
- (42) Moudens, A.; Georges, R.; Goubet, M.; Makarewicz, J.; Loksh-tanov, S. E.; Vigasin, A. A. *J. Chem. Phys.* **2009**, *131*, No. 204312.
- (43) Caminati, W.; Moreschini, P.; Rossi, I.; Favero, P. G. *J. Am. Chem. Soc.* **1998**, *120*, 11144.
- (44) Georgiou, A. S.; Legon, A. C.; Millen, D. J. *Proc. R. Soc. London, Ser. A* **1981**, *373*, 511.
- (45) Legon, A. C.; Wallwork, A. L.; Millen, D. J. *Chem. Phys. Lett.* **1991**, *178*, 279.
- (46) Gross, M.; Herman, G.; Scharman, A. *Spectrochim. Acta, Part B* **1989**, *44*, 597.
- (47) Petry, R.; Klee, S.; Lock, M.; Winnewisser, B. P.; Winnewisser, M. *J. Mol. Struct.* **2002**, *612*, 369.
- (48) Herman, M.; Didriche, K.; Hurtmans, D.; Kizil, B.; Macko, P.; Rizopoulos, A.; Van Poucke, P. *Mol. Phys.* **2007**, *105*, 815.
- (49) Thiévin, J. Thèse de doctorat de l'université Rennes I, 2007.
- (50) Grimme, S. *J. Chem. Phys.* **2006**, *124*, No. 034108.
- (51) Frisch, M. J.; Trucks, G. W.; Schlegel, H. B.; Scuseria, G. E.; Robb, M. A.; Cheeseman, J. R.; Scalmani, G.; Barone, V.; Mennucci, B.; Petersson, G. A.; Nakatsuji, H.; Caricato, M.; Li, X.; Hratchian, H. P.; Izmaylov, A. F.; Bloino, J.; Zheng, G.; Sonnenberg, J. L.; Hada, M.; Ehara, M.; Toyota, K.; Fukuda, R.; Hasegawa, J.; Ishida, M.; Nakajima, T.; Honda, Y.; Kitao, O.; Nakai, H.; Vreven, T.; Montgomery, J. A., Jr.; Peralta, J. E.; Ogliaro, F.; Bearpark, M.; Heyd, J. J.; Brothers, E.; Kudin, K. N.; Staroverov, V. N.; Kobayashi, R.; Normand, J.; Raghavachari, K.; Rendell, A.; Burant, J. C.; Iyengar, S. S.; Tomasi, J.; Cossi, M.; Rega, N.; Millam, J. M.; Klene, M.; Knox, J. E.; Cross, J. B.; Bakken, V.; Adamo, C.; Jaramillo, J.; Gomperts, R.; Stratmann, R. E.; Yazyev, O.; Austin, A. J.; Cammi, R.; Pomelli, C.; Ochterski, J. W.; Martin, R. L.; Morokuma, K.; Zakrzewski, V. G.; Voth, G. A.; Salvador, P.; Dannenberg, J. J.; Dapprich, S.; Daniels, A. D.; Ö. Farkas, Foresman, J. B.; Ortiz, J. V.; Cioslowski, J.; Fox, D. J. *Gaussian 09, Revision A.02*; Gaussian, Inc.: Wallingford, CT, 2009.
- (52) MOLPRO is a package of ab initio programs written by Werner, H.-J.; Knowles, P. J.; Lindh, R.; Manby, F. R.; M. Schütz, Celani, P.; Korona, T.; Mitrushenkov, A.; Rauhut, G.; Adler, T. B.; Amos, R. D.; Bernhardsson, A.; Berning, A.; Cooper, D. L.; Deegan, M. J. O.; Dobbyn, A. J.; Eckert, F.; Goll, E.; Hampel, C.; Hetzer, G.; Hrenar, T.; Knizia, G.; C. Köppl, Liu, Y.; Lloyd, A. W.; Mata, R. A.; May, A. J.; McNicholas, S. J.; Meyer, W.; Mura, M. E.; Nicklass, A.; Palmieri, P.; K. Pflüger, Pitzer, R.; Reiher, M.; Schumann, U.; Stoll, H.; Stone, A. J.; Tarroni, R.; Thorsteinsson, T.; Wang, M.; Wolf, A.; .
- (53) Frisch, M. J.; Pople, J. A.; Binkley, J. S. *J. Chem. Phys.* **1984**, *80*, 3265.
- (54) Dunning, T. H., Jr. *J. Chem. Phys.* **1989**, *90*, 1007.
- (55) Goubet, M.; Asselin, P.; Manceron, L.; Soulard, P.; Perchard, J. P. *Phys. Chem. Chem. Phys.* **2003**, *5*, 3591.
- (56) Goubet, M.; Asselin, P.; Soulard, P.; Perchard, J. P. *Phys. Chem. Chem. Phys.* **2003**, *5*, 5365.
- (57) Bouteiller, Y.; Perchard, J. P. *Chem. Phys.* **2004**, *305*, 1.
- (58) Ceponkus, J.; Karlström, G.; Nelander, B. *J. Phys. Chem. A* **2005**, *109*, 7859.
- (59) D. A. Mc Quarrie, *Statistical Thermodynamics*; Harper & Row: New York, 1973.
- (60) Vaida, V.; Headrick, J. E. *J. Phys. Chem. A* **2000**, *104*, 5401.
- (61) Tsuge, M.; Tsuji, K.; Kawai, A.; Shibuya, K. *J. Phys. Chem. A* **2007**, *111*, 3540.